Infrared Spectra of OMCO (M = Cr−Ni), $OMCO^-$ (M = Cr−Cu), and MCO_2^- (M = Co−Cu) in Solid Argon

Mingfei Zhou, Binyong Liang, and Lester Andrews*

Department of Chemistry, University of Virginia, Charlottesville, Virginia 22901

Received: November 17, 1998; In Final Form: January 20, 1999

Laser-ablated late transition metal atoms Cr through Ni react with CO_2 molecules to give the insertion products OMCO, which have been isolated in solid argon. The insertion $OMCO^-$ molecular anions (Cr through Cu) were formed by electron capture and/or reaction with CO_2^-, and the addition MCO_2^- anions (M = Co, Ni, Cu) were produced by direct reaction with CO_2^-. The excellent agreement between the observed frequencies and isotopic frequency ratios with those calculated by density functional theory supports these assignments.

Introduction

Carbon dioxide is a naturally abundant carbon source that has been implicated as a contributor to the greenhouse effect. The possibility of using CO_2 to synthesize useful chemical compounds has received considerable attention.[1−4] The interaction of CO_2 and transition metal centers has been studied both experimentally[5−12] and theoretically.[13−18] The interaction of thermally generated first-row transition metal atoms with CO_2 has been studied in a pure CO_2 matrix,[7] and different coordination products were suggested. In an argon matrix,[12] no obvious product was observed for Ni + CO_2.

Recent investigations have shown that laser-ablated early first-row transition metal atoms Sc, Ti, and V react with CO_2 molecules to give primarily the insertion product, OMCO, while photoisomerization to form the side-bonded OM-(η^2-CO) isomer and photoionization to the $OMCO^+$ and $OMOC^+$ cations proceeds upon photolysis with different wavelengths.[19−21] In the chromium case, OCrCO and $O_2Cr(CO)_2$ have been characterized.[22] Here we report a study of the reaction of laser-ablated Mn through Zn atoms with CO_2 molecules. We will show that insertion to form OMCO is observed for all the first-row transition metal atoms except Cu and Zn. The insertion molecular anions $OMCO^-$ for Cr through Cu and addition anions MCO_2^- for Co, Ni, and Cu are also produced during sample deposition and trapped in solid argon matrix.

Experimental Details

The experimental methods for pulsed-laser ablation and matrix isolation FTIR investigation of new chemical species have been reported previously.[23,24] The 1064 nm fundamental of a Nd:YAG laser was focused on the rotating metal target to a spot about 0.2 mm, the ablated metal atoms and electrons were co-deposited with CO_2 molecules in excess argon on to a 11−12K CsI window at 2−4 mmol/h for 1−2 h. Typically, low laser power (3−5 mJ/pulse) was used, which favored the stabilization of anion species and eliminated cluster formation. Carbon dioxide (Matheson) and isotopic $^{13}C^{16}O_2$, $^{12}C^{18}O_2$ (Cambridge Isotopic Laboratories) and $^{12}C^{16}O_2 + {}^{13}C^{16}O_2$, $^{12}C^{16}O_2 + {}^{12}C^{18}O_2$, or $^{12}C^{16}O_2 + {}^{12}C^{16,18}O_2 + {}^{12}C^{18}O_2$ mixtures were used in different experiments. FTIR spectra were recorded on a Nicolet 750 spectrometer at 0.5 cm^{-1} resolution and 0.1 cm^{-1} accuracy using a liquid nitrogen cooled MCTB detector. Samples were annealed and subjected to photolysis using a medium-pressure mercury lamp (240−580 nm) and optical filters.

Results

Co-deposition of laser-ablated late transition metal atoms and electrons with CO_2 in excess argon at 11−12 K revealed strong CO_2 absorptions at 2344.8, 2339.0 cm^{-1} and 663.5, 661.9 cm^{-1}, weak CO absorption at 2138.2 cm^{-1}, CO_2^- and its CO_2 complex absorptions at 1657.0, 1652.7 cm^{-1},[25,26] very weak $C_2O_4^+$ absorption at 1274.0 cm^{-1},[27] and CO_4^- at 1891.5, 1257.0, and 691.1 cm^{-1}.[26,28] Sample annealing decreased the anion and cation absorptions and produced $C_2O_4^-$ absorptions at 1856.7 and 1184.7 cm^{-1}.[26] Photolysis decreased and destroyed the anion and cation absorptions. A weak band at 2037.1 cm^{-1}, increased on full-arc photolysis, is stronger with Cu and Zn and is in good agreement with the spectrum of CO_3 radical.[28] The above metal-independent bands were observed with all metals but are only listed in the table for Mn. Besides these common absorptions, new metal-dependent product absorptions were also observed for all metal systems Mn through Zn.

Mn. The spectra of laser-ablated Mn atoms co-deposited with 0.5% CO_2 in excess argon in selected regions are shown in Figure 1, and the absorptions are listed in Table 1. Sample deposition produced strong bands at 2082.5, 869.9 cm^{-1}, weak bands at 1810.0, 810.1 cm^{-1}, and MnO absorption at 833.3 cm^{-1}.[29] These bands slightly decreased on annealing, while photolysis doubled the 2082.5 and 869.9 cm^{-1} absorptions but destroyed the 1810.0 and 810.1 cm^{-1} bands. Photolysis and higher temperature annealing produced extra band sets at 2126.0, 2056.0, 993.8 cm^{-1} and 1755.4, 1077.0, 772.7 cm^{-1} and weak absorptions at 2173.0, 2097.3, 1929.9, 851.9 cm^{-1}.

Similar spectra were obtained using isotopic $^{13}C^{16}O_2$ and $^{12}C^{18}O_2$ samples, and the isotopic counterparts are listed in Table 1. Mixed $^{12}C^{16}O_2 + {}^{13}C^{16}O_2$ and $^{12}C^{16}O_2 + {}^{12}C^{16,18}O_2 + {}^{12}C^{18}O_2$ experiments were also done, and the mixed $^{12}C^{16}O_2 + {}^{13}C^{16}O_2$ spectra in selected regions are shown in Figure 2.

Fe. The spectra of laser-ablated iron atoms co-deposited with 0.5% CO_2 in excess argon in selected regions are shown in Figure 3, and the absorptions are listed in Table 2. Strong bands

10.1021/jp984439d CCC: $18.00
Published on Web 03/13/1999

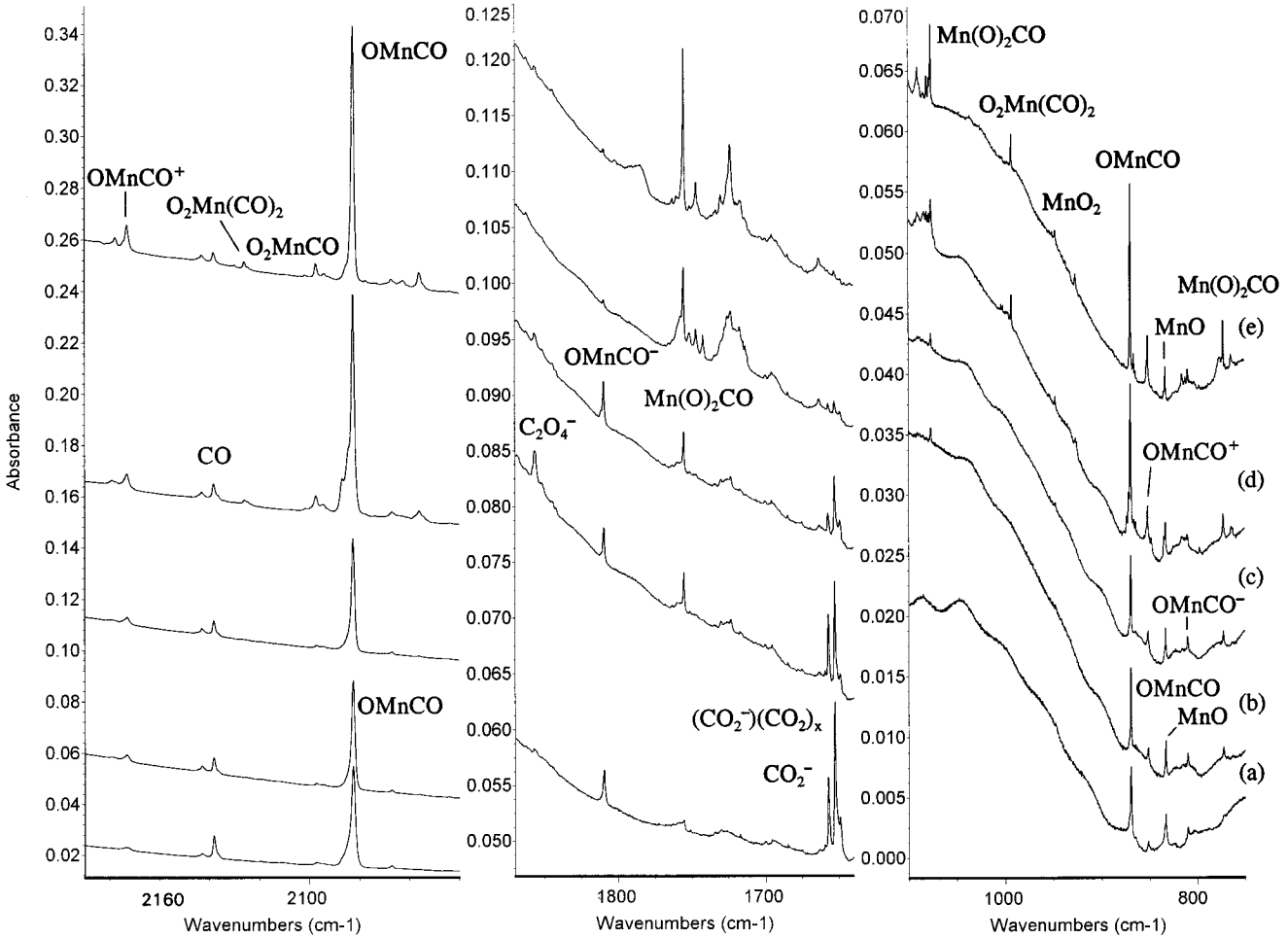

Figure 1. Infrared spectra in selected regions for reaction of laser-ablated Mn atoms with 0.5% CO_2 in excess argon during condensation at 12 K: (a) sample co-deposition for 1 h, (b) after annealing to 25 K, (c) after $\lambda > 470$ nm photolysis, (d) after full-arc photolysis, and (e) after annealing to 30 K.

at 2037.1 and 872.8 cm^{-1} observed after sample deposition slightly decreased on annealing but greatly increased on broadband photolysis. Weak associated bands at 1806.3 and 814.8 cm^{-1} appeared on deposition, remained unchanged on 20 and 25 K annealing, disappeared on photolysis, and did not reappear on further annealing to 30 K. A weak FeO_2 band was observed at 945.7 cm^{-1}.[30] Sharp band sets at 1767.8, 1031.5, 907.8, 793.6, 791.3 cm^{-1} and 2108.3, 1005.8 cm^{-1} were produced on photolysis and increased on annealing. Again, isotopic $^{13}C^{16}O_2$, $^{12}C^{18}O_2$ and mixed $^{12}C^{16}O_2 + {}^{13}C^{16}O_2$ and $^{12}C^{16}O_2 + {}^{12}C^{16,18}O_2 + {}^{12}C^{18}O_2$ experiments were done, and the results are also listed in Table 2.

Co. The spectra of laser-ablated Co-atom reactions with CO_2 in selected regions are shown in Figure 4, and the absorptions are listed in Table 3. Sample deposition revealed a sharp, strong band at 2026.6 cm^{-1} and a weak associated band at 783.8 cm^{-1}, which increased together on annealing and photolysis. Sample deposition also produced weak bands at 1849.2, 807.9 cm^{-1} and 1693.5,1228.4, 721.9 cm^{-1}. The 1849.2 and 807.9 cm^{-1} bands decreased on 25 K annealing, slightly increased on photolysis using a 470 nm long-wavelength pass filter, but disappeared on full-arc photolysis. The 1693.5, 1228.4, 721.9 cm^{-1} band set decreased on 25 K annealing and almost disappeared on photolysis using 470 nm long-wavelength pass filter. The CoO absorption at 846.2 cm^{-1} was observed after deposition, while the CoO_2 absorption at 945.2 cm^{-1} was produced on full-arc photolysis.[31] The $^{13}C^{16}O_2$ and $^{12}C^{18}O_2$ isotopic counterpart product absorptions are also listed in Table 3. Mixed isotopic experiments only produced pure isotopic counterparts.

Ni. Reaction of Ni with CO_2 gave a strong band at 2086.6 cm^{-1} and weak bands at 1881.4, 1684.8, 1226.1, and 723.9 cm^{-1} as shown in Figure 5. A weak NiO doublet was observed at 824.3, 821.4 cm^{-1}.[31] The 2086.6 cm^{-1} band remained the same on first 25 K annealing, increased 20% on full-arc photolysis, and increased 40% more on 30 K annealing. The 1881.4 cm^{-1} band slightly decreased on 25 K annealing, and slightly increased on photolysis using the 470 nm long-wavelength pass filter, and disappeared on full-arc photolysis. The 1684.8, 1226.1, and 723.9 cm^{-1} bands tracked together through all of the experiments; they slightly decreased on annealing to 25 K, decreased 50% on photolysis using a 470 nm long-wavelength pass filter, and disappeared on full-arc photolysis. The 1881.4 cm^{-1} band and 1684.8, 1226.1, 723.9 cm^{-1} band set did not reappear on further annealing. The $^{12}C^{16}O_2$ product absorptions and their isotopic $^{13}C^{16}O_2$ and $^{12}C^{18}O_2$ counterparts were listed in Table 4. Only pure isotopic counterparts were observed for all the product absorptions in mixed $^{12}C^{16}O_2 + {}^{13}C^{16}O_2$ and $^{12}C^{16}O_2 + {}^{12}C^{18}O_2$ experiments.

Cu. The Cu + CO_2 system produced weak absorption at 1943.4 cm^{-1} and a weak band set at 1713.4, 1234.2, and 697.0 cm^{-1}, which were slightly decreased on 25 K annealing and destroyed on full-arc photolysis. These bands shifted to 1896.9, 1667.9, 1220.7, 682.8 cm^{-1} in $^{13}C^{16}O_2$ spectra, and only doublets were observed in the mixed $^{12}C^{16}O_2 + {}^{13}C^{16}O_2$ product spectrum.

TABLE 1: Infrared Absorptions (cm^{-1}) from Co-depositing of Laser-Ablated Mn Atoms with CO_2 in Excess Argon at 10 K

$^{12}C^{16}O_2$	$^{13}C^{16}O_2$	$^{12}C^{18}O_2$	$^{12}C^{16}O_2 + ^{13}C^{16}O_2$	$^{12}C^{16}O_2 + ^{12}C^{16,18}O_2 + ^{12}C^{18}O_2$	*R*(12/13)	*R*(16/18)	assignment
2344.8	2279.2	2309.7	2344.8, 2279.2	2344.8, 2327.8, 2309.7	1.0288	1.0152	CO_2
2339.0	2273.6	2304.1	2339.0, 2273.6	2339.0, 2322.0, 2304.1	1.0288	1.0152	CO_2
2177.7	2129.3	2126.6	2177.8, 2129.3	2177.8, 2126.3	1.0227	1.0240	$OMnCO^+$ site
2173.0	2124.7	2122.1	2173.0, 2124.7	2172.9, 2122.1	1.0227	1.0240	$OMnCO^+$
2143.0	2095.8	2091.9	2143.0, 2095.8	2143.0, 2091.9	1.0225	1.0244	$(CO)_x$
2138.3	2091.3	2087.1	2138.3, 2091.3	2138.3, 2087.1	1.0225	1.0245	CO
2126.0	2077.7	2078.0	2126.0, 2109.0, 2077.7		1.0233	1.0231	$O_2Mn(CO)_2$
2097.3	2049.8	2049.6	2097.2, 2049.9	2097.2, 2049.6	1.0232	1.0233	O_2MnCO
2082.5	2036.5	2033.4	2082.6, 2036.6	2082.5, 2033.3	1.0226	1.0242	OMnCO
2056.0	2010.9	2007.4	2056.0, 2026.2, 2011.0	2056.1, 2024.2, 2007.6	1.0224	1.0242	$O_2Mn(CO)_2$
2037.1	1983.3				1.02713		CO_3
1929.9	1884.6	1888.4	1929.9, 1884.6	1929.8, 1884.5	1.0240	1.0220	$OMn(CO)_2$
1891.5	1831.6	1863.3			1.0328	1.0151	CO_4^-
1856.7	1806.4	1826.8	1856.9, 1806.7		1.0279	1.0164	$C_2O_4^-$
1810.0	1767.7	1771.0	1810.0, 1767.7	1809.9, 1770.9	1.0239	1.0220	$OMnCO^-$
1755.4	1716.1	1718.0	1755.5, 1716.2	1755.2, 1718.1	1.0229	1.0218	$Mn(O)_2CO$
1723.7							$Mn(O)_2CO$ site
1657.0	1612.9	1629.3	1657.0, 1612.9	1657.0, 1643.9, 1629.3	1.0273	1.0170	CO_2^-
1652.7	1608.8	1625.0	1652.7, 1608.8	1652.7, 1639.8, 1625.0	1.0273	1.0171	$(CO_2^-)(CO_2)_x$
1383.9	1368.3	1339.2	1383.8, 1368.6	1383.8, 1359.4, 1339.3	1.0114	1.0334	$(CO_2)_x$
1279.0	1255.9	1227.7	1278.3, 1256.0	1278.4, 1254.6, 1227.7	1.0184	1.0418	$(CO_2)_x$
1274.0	1264.8	1221.7	1273.8, 1268.3, 1264.7		1.0073	1.0428	$C_2O_4^+$
1257.0	1248.2	1200.2			1.0071	1.0473	CO_4^-
1184.7	1177.3	1130.5	1184.7, 1180.6, 1177.0	1168.3, 1157.1, 1148.4, 1141.3	1.0063	1.0479	$C_2O_4^-$
1090.9	1063.1	1058.6			1.0262	1.0305	$Mn(O)_2CO$ site
1077.0	1049.1	1058.6	1077.1, 1049.1	1076.9, 1076.2, 1069.4, 1068.1, 1060.4, 1058.8	1.0266	1.0174	$Mn(O)_2CO$
993.8	993.8	956.9		993.8980.1, 957.0		1.0386	$O_2Mn(CO)_2$
948.0	948.0						MnO_2
926.7	922.6	877.7			1.0044	1.0558	$Mn(O)_2CO$
869.9	870.1	832.7		869.9, 832.8		1.0447	OMnCO
851.9	851.9	814.8		852.0, 814.7		1.0455	$OMnCO^+$
833.2	833.2	796.6		833.2, 796.6		1.0460	MnO
810.1	810.1	776.7		810.1, 777.0		1.0430	$OMnCO^-$
772.7	771.0	734.8	772.7, 771.0	772.7, 767.6, 756.3, 752.0, 739.0, 735.2	1.0022	1.0516	$Mn(O)_2CO$
691.1	681.1	670.2	691.2, 681.1		1.0147	1.0312	CO_4^-
663.5	644.6	653.5	663.5, 644.6	663.5, 658.5, 653.5	1.0293	1.0153	CO_2
661.9	643.2	651.9	661.9, 643.2	661.9, 656.9, 651.9	1.0291	1.0153	CO_2

TABLE 2: Infrared Absorptions (cm^{-1}) from Co-depositing Laser-Ablated Fe Atoms with CO_2 Molecules in Excess Argon at 10 K

$^{12}C^{16}O_2$	$^{13}C^{16}O_2$	$^{12}C^{18}O_2$	$^{12}C^{16}O_2 + ^{13}C^{16}O_2$	$^{12}C^{16}O_2 + ^{12}C^{18}O_2$	*R*(12/13)	*R*(16/18)	assignment
2108.2	2061.5	2059.0	2108.2, 2061.7	2108.2, 2059.0	1.0227	1.0239	O_2FeCO
2079.1	2033.3	2029.7		2079.1, 2029.7	1.0225	1.0243	$(OFeOCO^+)$
2037.1	1991.4	1989.2	2036.9, 1991.4	2037.1, 1989.2	1.0229	1.0241	OFeCO
1988.1	1943.1	1944.5		1988.1, 1944.5	1.0232	1.0224	$(OFe(CO)_2)$
1806.3	1763.3	1768.7	1806.4, 1763.3	1806.2, 1768.7	1.0244	1.0213	$OFeCO^-$
1767.8	1723.3	1729.1	1767.8, 1723.3	1767.8, 1729.1	1.0258	1.0224	$Fe(O)_2CO$
1031.5	1006.0	1013.2	1031.5, 1006.0	1031.5, 1030.2, 1023.9, 1022.5, 1014.9, 1013.2	1.0253	1.0181	$Fe(O)_2CO$
1005.9	1005.9	968.9		1005.9, 991.3, 968.9		1.0382	O_2FeCO
945.7	945.7	911.2		945.7, 930.8, 911.2		1.0379	FeO_2
907.8	904.9	861.0		900.1, 890.6, 879.0, 866.2	1.0032	1.0544	$Fe(O)_2CO$
885.6	885.6	846.8		885.6, 846.8		1.0458	$(FeOCO^+)$
872.8	872.8	834.8		872.8, 834.8		1.0455	OFeCO, FeO
870.3	870.3	832.1		870.3, 832.1		1.0459	site
814.8	814.8	781.3		814.7, 781.3		1.0429	$OFeCO^-$
793.6	769.2	782.8			1.0317	1.0138	$Fe(O)_2CO$
791.3	789.0				1.0029		$Fe(O)_2CO$

Zn. The Zn + CO_2 system produced metal-dependent bands at 2229.5 and 2084.4 cm^{-1}, which shifted to 2179.2 and 2035.7 cm^{-1} with $^{13}CO_2$. The former band increased on 25 K annealing, did not change on $\lambda > 470$ nm photolysis, diminished 80% on full-arc photolysis and increased on 35 K annealing whereas the 2084.4 cm^{-1} band decreased slightly on 25 K annealing and disappeared on $\lambda > 470$ nm photolysis.

Cr. The reaction of laser-ablated Cr atoms with CO_2 molecules has been reported earlier using relatively higher laser power.[22] Experiments with the Cr + CO_2 reaction were repeated here using relatively lower laser power, which favored the stabilization of anion species. The absorptions observed before for OCrCO, $O_2Cr(CO)_2$, and O_2CrCO were also produced here. Meanwhile, weak new absorptions at 1831.1 and 825.5 cm^{-1} were observed. These two bands decreased slightly on 25 K annealing, increased slightly on photolysis with $\lambda > 470$ nm radiation, and disappeared on full-arc photolysis. In $^{13}C^{16}O_2$ and $^{12}C^{18}O_2$ spectra, these two bands shifted to 1788.8, 824.4 cm^{-1} and 1790.7, 791.5 cm^{-1}, respectively.

CCl_4 Doping. Experiments were done with different concentrations of CCl_4 added to serve as an electron trap. Using the same experimental conditions, the initial spectra of the deposited sample with 0.05% CCl_4 added showed the CO_2^- absorption at 1652.7 cm^{-1} and $(CO_2)_xCO_2^-$ complex band at 1652.7 cm^{-1} to be more than 10-fold weaker, and experiments with 0.1% CCl_4 added totally eliminated the 1657.0 and 1652.7 cm^{-1} bands.[26] In both investigations, no $C_2O_4^-$ absorptions were produced at 1856.7 and 1184.7 cm^{-1} on annealing. All the absorptions in different metal systems, which will be assigned

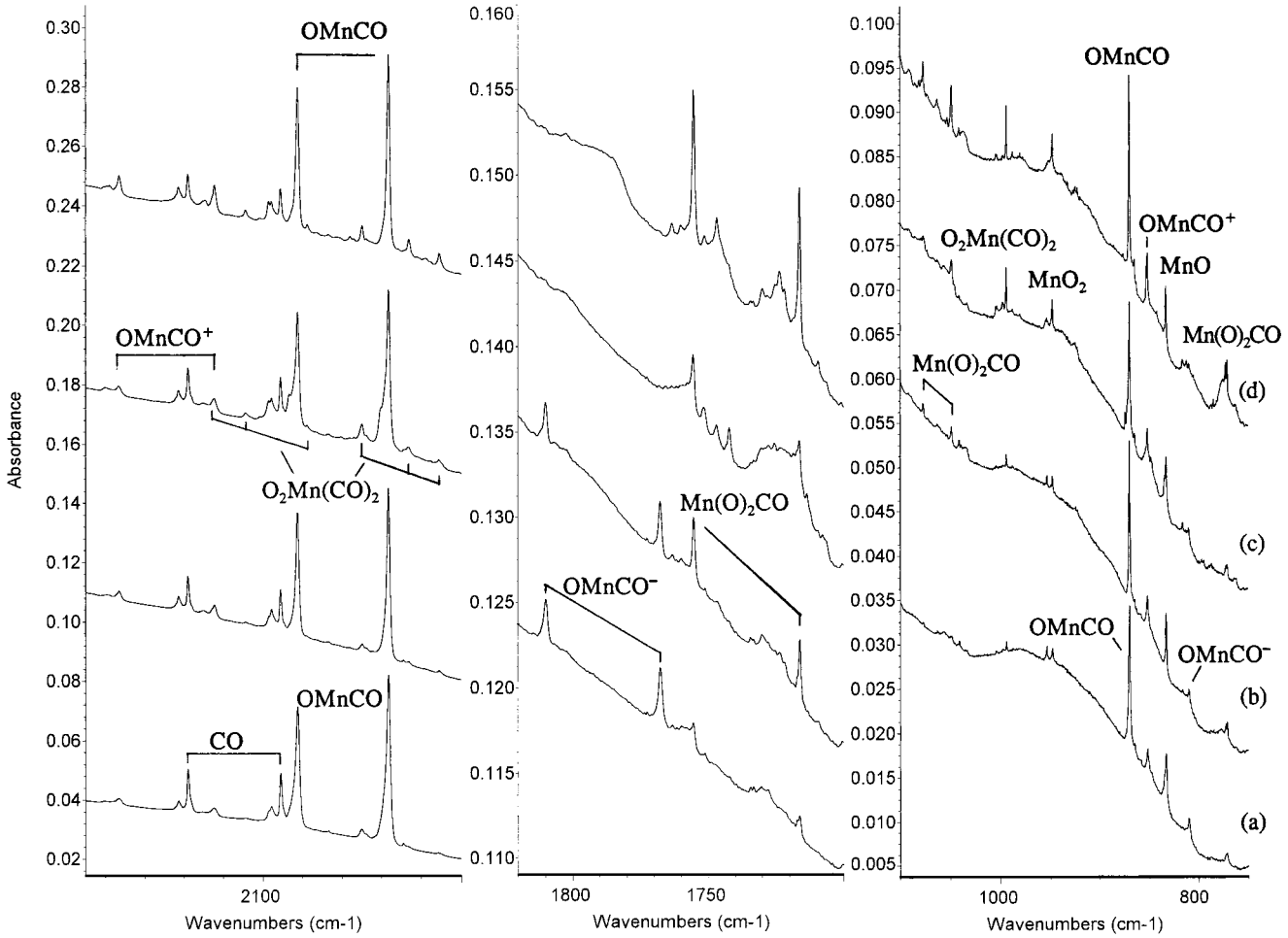

Figure 2. Infrared spectra in selected regions for reaction of laser-ablated Mn atoms with 0.4% $^{12}C^{16}O_2$ + 0.4%$^{13}C^{16}O_2$ in excess argon during condensation at 12 K: (a) sample co-deposition for 1 h, (b) after annealing to 25 K, (c) after full-arc photolysis, and (d) after annealing to 30 K.

TABLE 3: Infrared Absorptions (cm^{-1}) from Co-depositing of Laser-Ablated Co Atoms with CO_2 in Excess Argon at 10 K

$^{12}C^{16}O_2$	$^{13}C^{16}O_2$	$^{12}C^{18}O_2$	$^{12}C^{16}O_2 + {}^{13}C^{16}O_2$	*R*(12/13)	*R*(16/18)	assignment
2097.5	2050.0	2049.8		1.02317	1.02327	
2095.0	2047.6	2047.4		1.02315	1.02325	
2081.6	2036.0	2031.9	2081.7, 2036.0	1.02240	1.02446	($CoOCO^+$)
2026.6	1980.7	1980.7	2026.6, 1989.8	1.02317	1.02317	OCoCO
2018.8	1973.1	1973.1	2018.8, 1973.1	1.02316	1.02316	OCoCO site
2015.3	1969.5	1969.7	2015.2, 1969.6	1.02325	1.02315	OCoCO site
1971.7	1926.1	1929.3		1.02367	1.02198	
1849.2	1805.6	1810.7	1849.3, 1806.7	1.02415	1.02126	$OCoCO^-$
1693.5	1649.3			1.02680		$CoCO_2^-$
1228.4	1214.5	1180.9	1228.2, 1214.5	1.01146	1.04022	$CoCO_2^-$
945.2	945.2	910.9			1.03766	OCoO
909.3	909.3	875.5			1.03861	
854.1	854.0	816.2			1.04643	($CoOCO^+$)
846.1	846.1	808.6			1.04638	CoO
844.6	844.6	807.1			1.04646	CoO site
807.9	806.9	774.0		1.00124	1.04380	$OCoCO^-$
783.8	783.7	750.5			1.04437	OCoCO
721.9	707.5	701.1	721.8, 707.4	1.02035	1.02967	$CoCO_2^-$

to anion products, were totally eliminated, while weak absorptions due to CCl_3^+ and CCl_3 were observed.[32,33]

Calculations. Density functional calculations were performed for the product molecules expected here using the Gaussian 94 program.[34] The BP86 functional,[35] the 6-311+G* basis sets for C and O atoms,[36] and the set of Wachters and Hay as modified by Gaussian 94 for metal atoms[37] were used. Five MCO_2 isomers were calculated, namely, inserted OMCO, M[CO]O (η^2-*C,O* coordination), MCO_2 (η^1-*C* coordination), M[OO]C (η^2-*O*, *O*) coordination), and MOCO (η^1-*O* coordination). The calculated geometries, relative energies, vibrational frequencies, and intensities are listed in Tables 5−9 for Mn through Cu. For Mn, Fe, and Co, the inserted OMCO molecule was calculated to be the most stable isomer, followed by the M[CO]O and MCO_2 isomers, which were slightly higher in energy. Bridged Ni[CO]O was the most stable isomer and then $NiCO_2$ and ONiCO. For Cu, $CuCO_2$ was the most stable isomer, followed by the OCuCO molecule. The M[OO]C and MOCO isomers were higher in energy or converged to M + CO_2. Our results are different from restricted Hartree−Fock calculations

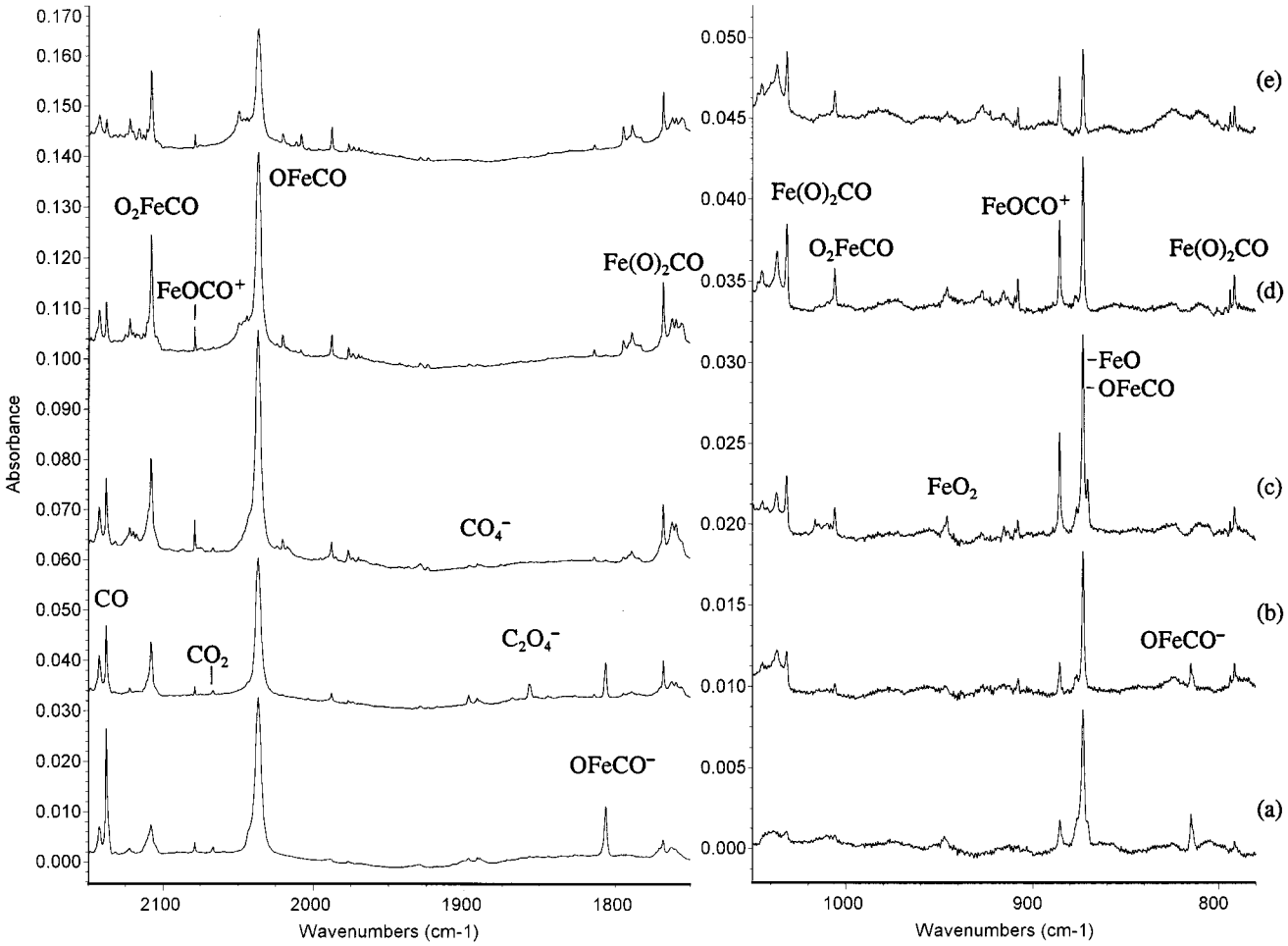

Figure 3. Infrared spectra in selected regions for reaction of laser-ablated Fe atoms with 0.5% CO_2 in excess argon during condensation at 12 K: (a) sample co-deposition for 1 h, (b) after annealing to 25 K, (c) after full-arc photolysis, (d) after annealing to 30 K, and (e) after annealing to 35 K.

TABLE 4: Infrared Absorptions (cm^{-1}) from Co-deposition of Laser-Ablated Ni Atoms with CO_2 in Excess Argon at 10 K

$^{12}C^{16}O_2$	$^{13}C^{16}O_2$	$^{12}C^{18}O_2$	$^{12}C^{16}O_2 + {}^{12}C^{18}O_2$	*R*(12/13)	*R*(16/18)	assignment
2086.6	2039.6	2038.6	2086.6, 2038.5	1.02304	1.02355	ONiCO
2072.7	2025.7	2025.4	2072.7, 2025.2	1.02320	1.02335	ONiCO site
1881.4	1836.8	1842.4	1881.4, 1842.2	1.02428	1.02117	$ONiCO^-$
1684.8	1641.9	1656.7	1684.8, 1656.7	1.02613	1.01696	$NiCO_2^-$
1226.1	1212.1	1180.4	1226.1, 1180.3	1.01155	1.03872	$NiCO_2^-$
835.5	835.3	798.9	835.4, 798.9		1.04581	X-NiO
824.3	824.3	788.1	824.3, 788.0		1.04593	^{58}NiO
821.4	821.4	785.1	821.0, 784.8		1.04624	^{60}NiO
723.9	709.4	703.1	723.8, 703.0	1.02044	1.02958	$NiCO_2^-$

reported by Jeung,[13] while the $NiCO_2$ isomer calculations are in reasonable agreement with those recently reported by Papai et al.[18]

Similar calculations were done on MCO_2^- anion isomers. Two forms, namely, $OMCO^-$ and MCO_2^-, were calculated, and the results are also listed in Tables 5−9. The $OMCO^-$ form was more stable than MCO_2^- for Mn, Fe, Co, and Ni, while for Cu, the $CuCO_2^-$ form was slightly lower in energy than $OCuCO^-$. Calculations were performed on two MCO_3 isomers for Mn and Fe, and the results are listed in Table 11. The O_2-MCO and $M(O)_2CO$ isomers were calculated to be very close in energy.

Discussion

The inserted OMCO molecules, $OMCO^-$ and MCO_2^- anions, MCO_3 isomers, and several cation species will be identified from isotopic shifts and DFT calculations.

OMCO. Reaction of Mn, Fe, CO, and Ni atoms with CO_2 molecules revealed strong absorptions in the 2000−2100 cm^{-1} region. (Mn, 2082.5 cm^{-1}; Fe, 2037.1 cm^{-1}; Co, 2026.6 cm^{-1}; Ni, 2086.6 cm^{-1}). These bands were the strongest absorptions on sample deposition and increased on broadband photolysis. The carbon-12/13 isotopic ratios (between 1.0226 and 1.0232) and oxygen-16/18 ratios (between 1.0232 and 1.0242) were higher and lower, respectively, than diatomic CO ratios, which indicate that the C atom is vibrating between O and another mass. The doublet isotopic structures in mixed $^{12}C^{16}O_2 + {}^{13}C^{16}O_2$ and $^{12}C^{16}O_2 + {}^{12}C^{18}O_2$ or $^{12}C^{16}O_2 + {}^{12}C^{16,18}O_2 + {}^{12}C^{18}O_2$ experiments confirmed that only one CO subunit is involved in this vibrational mode. In the lower region, bands at 869.9, 872.8, and 783.8 cm^{-1} for Mn, Fe, and Co tracked with the upper absorptions. These bands showed very small or no carbon-13 isotopic shifts and large oxygen isotopic shifts. The oxygen isotopic ratios indicate that these are terminal M−O

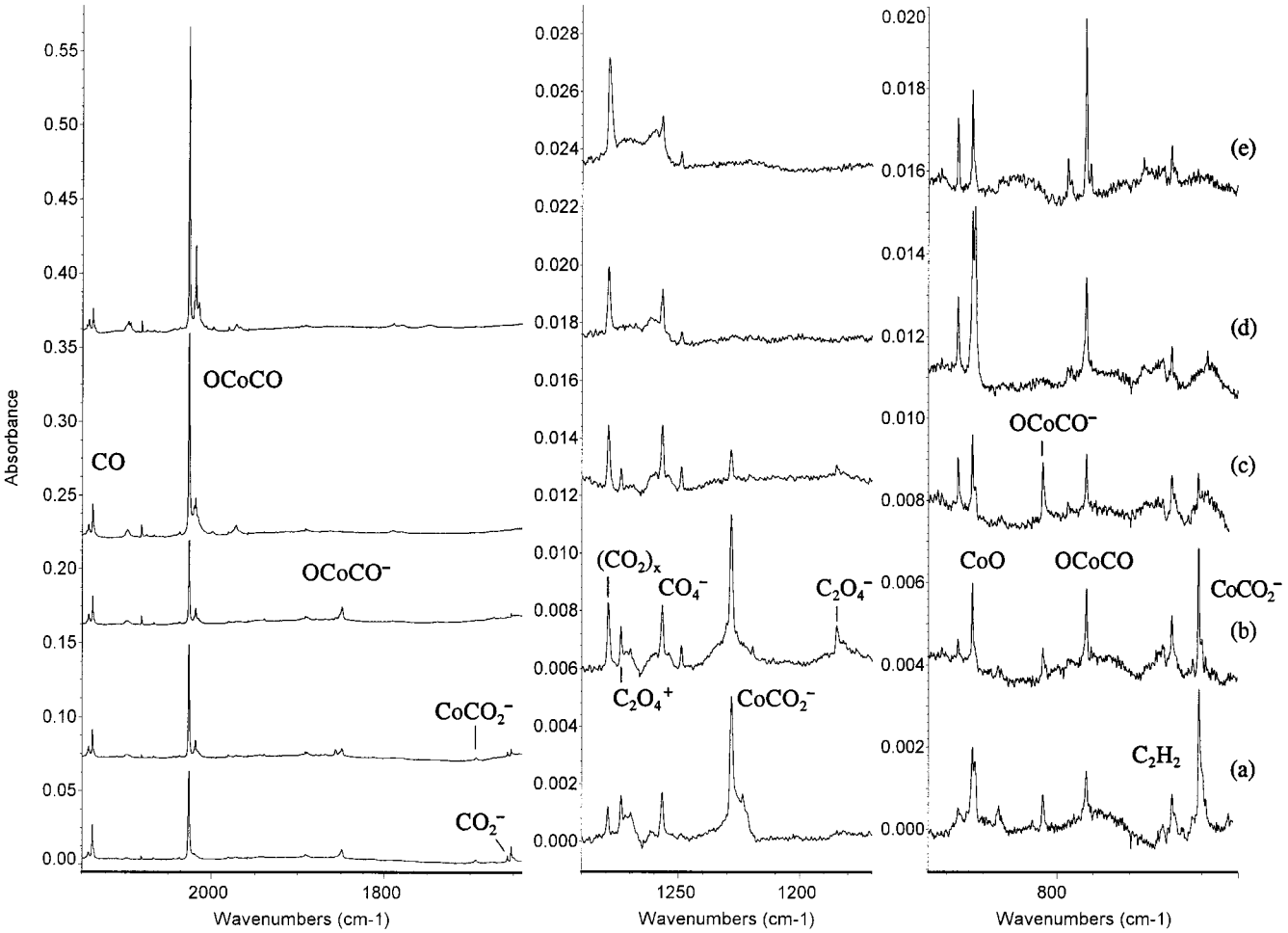

Figure 4. Infrared spectra in selected regions for reaction of laser-ablated Co atoms with 0.5% CO_2 in excess argon during condensation at 12 K: (a) sample co-deposition for 1 h, (b) after annealing to 25 K, (c) after $\lambda > 470$ nm photolysis, (d) after full-arc photolysis, and (e) after annealing to 30 K.

TABLE 5: Calculated Geometries, Relative Energies (kcal/mol), Vibrational Frequencies (cm^{-1}), and Intensities (km/mol) for $MnCO_2$ Isomers

molecule	relative energy	geometry	frequency (intensity)
OMnCO($^6\Sigma^+$)	0	Mn−O: 1.639 Å, Mn−C: 2.00 Å, C−O: 1.152 Å, linear	2026.7(798), 901.0(121), 363.0(14), 339.1(0), 339.1(0), 94.3(15), 94.3(15)
Mn[OC]O′ (^{6}A′)	+4.8	Mn−O: 2.094 Å, Mn−C: 2.058 Å, C−O: 1.268 Å, C−O′: 1.201 Å, ∠OCO′: 143.7°	1868.1(443), 1130.8(231), 654.6(307), 448.5(1), 323.4(6), 213.3(6)
OMnCO (^{4}A″)	+6.7	Mn−O: 1.597 Å, Mn−C: 1.823 Å, C−O: 1.164 Å, ∠OMnC: 105.8°, ∠MnCO: 176.1°	1979.7(707), 951.5(130), 509.8(3), 387.4(3), 344.6(2), 141.3(12)
$MnCO_2$ ($^6A_1$)	+9.6	Mn−C: 2.059 Å, C−O: 1.225 Å, ∠OCO: 147.4°	1867.6(304), 1201.9(279), 672.0(288), 444.8(2), 240.0(11), 156.3i(5)
Mn[OO]C ($^6A_1$)	+19.2	Mn−O: 2.110 Å, C−O: 1.272 Å, ∠OCO: 123.8°	1442.0(302), 1168.5(207), 642.5(171), 351.0(3), 265.5(3), 258.6(5)
Mn[OC]O′ (^{4}A″)	+20.8	Mn−O: 1.816 Å, Mn−C: 1.883 Å, C−O: 1.352 Å, C−O′: 1.203 Å, ∠OCO′: 136.1°	1782.1(617), 920.1(109), 693.6(61), 474.8(7), 456.5(0), 311.1(8)
Mn[OO]C ($^8A_1$)	+33.7	Mn−O: 2.203 Å, C−O: 1.263 Å, ∠OCO: 126.7°	1501.9(260), 1296.7(24), 751.8(54), 304.4(74), 243.0(1), 147.6(8)
MnOCO (^{8}A′)	+34.4	Mn−O: 1.929 Å, O−C: 1.319 Å, C−O: 1.203 Å, ∠MnOC: 140.0°, ∠OCO: 129.9°	1738.3(559), 1141.0(406), 704.3(36), 357.0(68), 55.1(0), 39.3(1)
$MnCO_2$ ($^8A_1$)	+48.3	Mn−C: 2.271 Å, C−O: 1.237 Å, ∠OCO: 143.2°	1727.0(274), 1197.5(47), 677.5(10), 232.4(41), 198.7(20), 173.5i(1)
$OMnCO^-$ (^{5}A″)	−39.1	Mn−O: 1.674 Å, Mn−C: 1.858 Å, C−O: 1.197 Å, ∠OMnC: 149.9°, ∠MnCO: 171.8°	1783.8(918), 833.0(238), 472.8(2), 377.4(11), 377.1(2), 83.3(7)
$OMnCO^-$ (^{3}A″)	−32.6	Mn−O: 1.638 Å, Mn−C: 1.762 Å, C−O: 1.207 Å, ∠OMnC: 118.6°, ∠MnCO: 168.5°	1743.6(1222), 865.3(224), 564.7(0.4), 423.0(12), 399.0(4), 139.3(3)
$OMnCO^+$ (^{5}A′)	+200.5	Mn−O: 1.594 Å, Mn−C: 2.037 Å, C−O: 1.129 Å, ∠O−Mn−C: 98.8°, ∠Mn−C−O: 175.9°	2204.3(148), 967.1(51), 348.5(1), 323.8(2), 276.7(1), 105.3(17)

stretching vibrations. Similar to bands for OScCO, OTiCO, and OVCO, these bands are suitable for assignment to C−O and M−O stretching vibrations of the inserted OMCO molecules.

The OMCO assignments are further supported by DFT calculations. As mentioned, the inserted OMCO molecules are the most stable MCO_2 isomers for Mn, Fe, and Co while for Ni ONiCO is slightly higher than the Ni[CO]O molecule. As shown in Table 10, the calculated C−O stretching and M−O stretching vibrational frequencies and isotopic frequency ratios were very close to the observed values. Finally, note that the calculated M−O stretching vibration is weaker than the corresponding C−O stretching vibration from Mn through Cu, so for ONiCO, we cannot observe the Ni−O stretching vibration.

The OMCO molecules were most likely formed by insertion

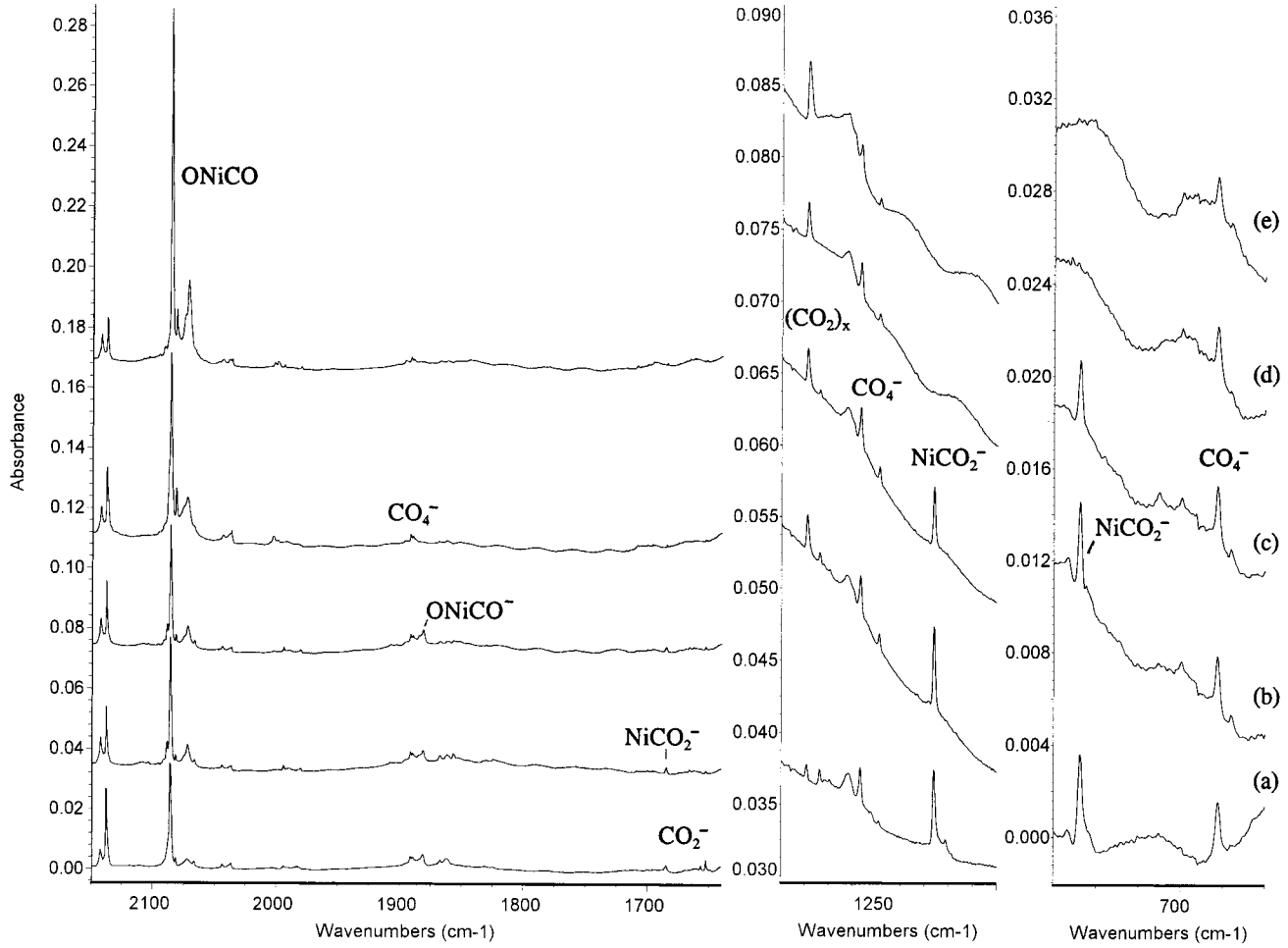

Figure 5. Infrared spectra in selected regions for reaction of laser-ablated Ni atoms with 0.5% CO_2 in excess argon during condensation at 12 K: (a) sample co-deposition for 1 h, (b) after annealing to 25 K, (c) after $\lambda > 470$ nm photolysis, (d) after full-arc photolysis, and (e) after annealing to 30 K.

TABLE 6: Calculated Geometries, Relative Energies (kcal/mol), Vibrational Frequencies (cm^{-1}), and Intensities (km/mol) for $FeCO_2$ Isomers

molecule	relative energy	geometry	frequency (intensity)
OFeCO ($^5A''$)	0	Fe−O: 1.626 Å, Fe−C: 1.891 Å, C−O: 1.155 Å, ∠OFeC: 143.1°, ∠FeCO: 169.6°	2017.8(751), 897.8(82), 429.5(17), 334.8(2), 330.3(1), 97.1(19)
OFeCO ($^3A''$)	+3.8	Fe−O: 1.597 Å, Fe−C: 1.751 Å, C−O: 1.166 Å, ∠OFeC: 109.6°, ∠FeCO: 168.0°	1980.9(688), 909.2(107), 562.5(5), 440.4(1), 380.8(1), 154.5(12)
Fe[OC]O′ ($^5A''$)	+8.8	Fe−O: 2.053 Å, Fe−C: 1.995 Å, C−O: 1.265 Å, C−O′: 1.197 Å, ∠OCO′: 146.0°	1900.9(440), 1112.2(248), 635.7(374), 477.9(1), 305.1(1), 206.1(3)
Fe[OC]O′ ($^3A''$)	+10.8	Fe−O: 1.838 Å, Fe−C: 1.885 Å, C−O: 1.304 Å, C−O′: 1.203 Å, ∠OCO′: 141.9°	1847.3(499), 1027.2(140), 695.3(122), 464.0(0), 455.0(14), 290.7(10)
$FeCO_2$ ($^5B_1$)	+12.7	Fe−C: 2.004 Å, C−O: 1.219 Å, ∠OCO: 151.3°	1922.1(286), 1178.6(258), 624.2(392), 510.5(1), 239.4(5), 147.6i(6)
Fe[OO]C ($^5A_1$)	+27.2	Fe−O: 2.034 Å, C−O: 1.270 Å, ∠OCO: 126.9°	1463.8(318), 1123.3(223), 604.1(225), 387.7(3), 288.3(2), 259.1(25)
FeOCO ($^7A'$)	+48.1	Fe−O: 1.885 Å, O−C: 1.327 Å, C−O: 1.201 Å, ∠FeOC: 129.3°, ∠OCO: 128.8°	1729.3(332), 1100.8(318), 715.5(29), 380.8(56), 73.9(0), 73.2(0)
$FeCO_2^-$ ($^4B_1$)	−29.2	Fe−C: 1.987 Å, C−O: 1.244 Å, ∠OCO: 137.9°	1701.6(273), 1186.5(622), 683.9(342), 507.5(0.2), 273.8(17), 37.2(5)
$OFeCO^-$ ($^4A''$)	−48.9	Fe−O: 1.670 Å, Fe−C: 1.761 Å, C−O: 1.200 Å, ∠OFeC: 137.9°, ∠FeCO: 167.9°	1788.4(1072), 815.0(217), 550.1(5), 466.6(4), 419.6(4), 123.5(8)

reaction 1 using energetic laser-ablated transition metal atoms.

$$M^* + CO_2 \rightarrow OMCO \quad (1)$$

The OMCO molecule absorptions increased on photolysis, indicating that reaction 1 can also be initiated by photolysis and that activation energy is required. As reported recently, thermal Ni atoms co-deposited with CO_2 molecules in an argon matrix failed to give any products.[12] In the present experiments, the OCoCO and ONiCO absorptions increased on 30 K annealing after photolysis, indicating that they can also be produced by reaction 2.

$$MO + CO \rightarrow OMCO \quad (2)$$

The OCoCO and ONiCO absorptions did not increase on annealing before photolysis, as CoO and NiO were not present. However, CoO and NiO were produced by photolysis, and OCoCO and ONiCO absorptions increased on annealing.

Although the Ni[CO]O isomer was calculated to be more stable than ONiCO, no evidence was found for this molecule. The inserted OCuCO molecule was calculated to be higher in energy than $CuCO_2$, and it was not observed here.

TABLE 7: Calculated Geometries, Relative Energies (kcal/mol), Vibrational Frequencies (cm^{-1}), and Intensities (km/mol) for $CoCO_2$ and $CoCO_2^-$ Isomers

molecule	relative energy	geometry	frequency (intensity)
OCoCO ($^4A''$)	0	Co−O: 1.624 Å, Co−C: 1.808 Å, C−O: 1.158 Å, ∠OCoC: 133.4°, ∠CoCO: 163.6°	2017.5(699), 853.4(42), 496.2(16), 400.3(1), 361.2(1), 123.7(14)
Co[OC]O′ ($^2A''$)	+2.3	Co−O: 1.829 Å, Co−C: 1.825 Å, C−O: 1.308 Å, C−O′: 1.197 Å, ∠OCO′: 142.1°	1846.0(508), 1023.8(96), 705.2(97), 473.5(0), 469.2(0), 296.1(7)
OCoCO ($^2A''$)	+5.5	Co−O: 1.612 Å, Co−C: 1.739 Å, C−O: 1.159 Å, ∠OCoC: 109.9°, ∠CoCO: 169.4°	2018.9(650), 883.1(52), 541.5(7), 361.4(0), 349.0(2), 135.4(8)
Co[OC]O′ ($^4A''$)	+6.4	Co−O: 2.179 Å, Co−C: 2.015 Å, C−O: 1.240 Å, C−O′: 1.197 Å, ∠OCO′: 150.1°	1956.8(372), 1158.9(245), 603.7(438), 558.8(0), 268.6(1), 162.6(6)
$CoCO_2$ ($^4B_1$)	+12.8	Co−C: 1.971 Å, C−O: 1.218 Å, ∠OCO: 151.0°	1924.7(281), 1182.0(252), 619.0(382), 496.8(2), 245.5(9), 73.6i(6)
Co[OO]C ($^4B_1$)	+28.6	Co−O: 2.054 Å, C−O: 1.254 Å, ∠OCO: 130.2°	1612.4(242), 1156.5(213), 612.7(148), 304.9(3), 267.1(3), 241.8(14)
$CoCO_2^-$ ($^3B_2$)	−38.8	Co−C: 1.982 Å, C−O: 1.240 Å, ∠OCO: 138.6°	1726.2(345), 1194.9(594), 680.1(354), 577.9(2), 268.2(14), 79.8i(2)
$OCoCO^-$ ($^3A''$)	−53.4	Co−O: 1.670 Å, Co−C: 1.727 Å, C−O: 1.191 Å, ∠OCoC: 133.7°, ∠CoCO: 165.3°	1838.0(1129), 803.3(198), 558.6(6), 453.1(2), 398.2(2), 132.4(5)

TABLE 8: Calculated Geometries, Relative Energies (kcal/mol), Vibrational Frequencies (cm^{-1}), and Intensities (km/mol) for $NiCO_2$ Isomers

molecule	relative energy	geometry	frequency (intensity)
Ni[OC]O′ ($^1A'$)	0	Ni−O: 1.841 Å, Ni−C: 1.850 Å, C−O: 1.277 Å, C−O′: 1.167 Å, ∠OCO′: 146.9°	1906.8(513), 1091.2(91), 684.5(142), 509.5(2), 493.8(1), 268.4(4)
$NiCO_2$ ($^1A_1$)	+14.2	Ni−C: 1.782 Å, C−O: 1.230 Å, ∠OCO: 151.9°	1844.0(492), 1162.1(219), 772.9(176), 498.0(3), 314.7(27), 292.1i(5)
ONiCO ($^3A''$)	+15.4	Ni−O: 1.677 Å, Ni−C: 1.799 Å, C−O: 1.152 Å, ∠ONiC: 140.6°, ∠NiCO: 168.0°	2054.9(749), 766.0(7), 467.2(21), 389.4(0), 341.1(0), 97.0(10)
Ni[OC]O′ ($^3A''$)	+18.4	Ni−O: 2.187 Å, Ni−C: 1.984 Å, C−O: 1.240 Å, C−O′: 1.167 Å, ∠OCO′: 150.6°	1958.3(381), 1154.2(221), 594.1(430), 513.7(1), 259.3(0), 114.6(6)
$NiCO_2$ ($^3A_2$)	+18.9	Ni−C: 2.019 Å, C−O: 1.212 Å, ∠OCO: 152.3°	1960.4(323), 1192.6(216), 596.0(415), 510.6(3), 231.9(0), 76.6i(3)
ONiCO ($^1A'$)	+32.1	Ni−O: 1.636 Å, Ni−C: 1.739 Å, C−O: 1.153 Å, ∠ONiC: 114.0°, ∠NiCO: 173.4°	2056.6(621), 836.8(37), 535.8(9), 369.6(2), 348.9(0), 116.9(9)
$NiCO_2^-$ ($^2A_1$)	−36.7	Ni−C: 1.866 Å, C−O: 1.248 Å, ∠OCO: 137.5°	1665.9(348), 1189.8(624), 729.4(265), 536.1(0), 296.8(18), 133.8i(4)
$ONiCO^-$ ($^2A'$)	−41.8	Ni−O: 1.698 Å, Ni−C: 1.725 Å, C−O: 1.185 Å, ∠ONiC: 154.9°, ∠NiCO: 172.0°	1875.0(1094), 736.4(35), 538.3(7), 438.0(0), 401.5(8), 105.8(8)

TABLE 9: Calculated Geometries, Relative Energies (kcal/mol), Vibrational Frequencies (cm^{-1}), and Intensities (km/mol) for $CuCO_2$ and $CuCO_2^-$ Isomers

molecule	relative energy	geometry	frequency (intensity)
$CuCO_2$ ($^2A_1$)	0	Cu−C: 2.181 Å, C−O: 1.198 Å, ∠OCO: 159.2°	2097.0(334), 1208.6(144), 555.0(3), 489.6(469), 87.5(23), 76.3(3)
OCuCO ($^2\Sigma^+$)	+24.5	O−Cu: 1.749 Å, Cu−C: 1.803 Å, C−O: 1.146 Å, linear	2097.4(638), 647.0(4), 440.3(15), 420.5(2), 367.2(0), 89.3(10), 75.4(15)
$CuCO_2^-$($^1A_1$)	−52.7	Cu−C: 2.005 Å, C−O: 1.236 Å, ∠OCO: 138.6°	1762.2(333), 1197.6(628) 667.1(455), 536.6(0), 257.2(1), 198.6(10)
$OCuCO^-$($^1\Sigma^+$)	−36.5	O−Cu: 1.694 Å, Cu−C: 1.748 Å, C−O: 1.18 Å, linear	1906.4(1035), 808.5(97), 497.9(3), 479.1(4), 479.1(4), 105.9(13), 105.9(13)
$CuOCO^-$($^1A'$)	−32.6	Cu−O: 2.192 Å, O−C: 1.222 Å, C−O: 1.206 Å, ∠CuOC: 121.9°, ∠OCO: 149.5°	1967.9(459), 1151.0(529), 496.0(728), 410.5(2), 121.6(24), 50.4(52)

$OMCO^-$. On sample deposition, weak bands were observed in the 1800−2100 cm^{-1} region for all of the metal systems studied here: Cr, 1831.1 cm^{-1}; Mn, 1856.7 cm^{-1}; Fe, 1806.2 cm^{-1}; Co, 1849.2 cm^{-1}; Ni, 1881.4 cm^{-1}; Cu, 1943.4 cm^{-1}; and Zn, 2084.4 cm^{-1}. All of these bands decreased slightly on annealing, increased on photolysis using a 470 nm long-wavelength pass filter, and disappeared on full-arc photolysis. The isotopic 12/13 ratios varied from 1.0237 to 1.0245 and the 16/18 ratios from 1.0212 to 1.0226. The doublet isotopic structures in mixed $^{12}C^{16}O_2 + {}^{13}C^{16}O_2$ and $^{12}C^{16}O_2 + {}^{12}C^{18}O_2$ or $^{12}C^{16}O_2 + {}^{12}C^{16,18}O_2 + {}^{12}C^{18}O_2$ experiments confirmed that these absorptions are due to terminal C−O stretching vibrations. For Cr, Mn, Fe, and Co, absorptions at 825.5, 810.1, 814.8, and 807.9 cm^{-1} tracked with the upper bands. The lower bands showed small or zero isotopic carbon-13 shifts and large oxygen isotopic shifts. The isotopic 16/18 ratios indicated that these are terminal M−O stretching vibrations. Again, the mixed isotopic doublet structures confirmed the involvement of only one O atom. Therefore, another species with the MCO_2 stoichiometry must be considered.

The photolysis behavior and CCl_4-doped experiments indicate that these absorptions are due to $OMCO^-$ anions. With CCl_4 present, electrons are preferentially captured by CCl_4 and the $OMCO^-$ bands are eliminated from the product spectrum. DFT calculation confirmed the $OMCO^-$ assignments. As listed in Table 10, the calculated vibrational frequencies and isotopic frequency ratios were in excellent agreement with the observed values. For $ONiCO^-$, $OCuCO^-$, and $OZnCO^-$, the Ni−O, Cu−O, and Zn−O stretching vibrations were calculated to be very weak compared to the C−O stretching mode, and these bands are not observed here.

The C−O stretching frequencies of $OCrCO^-$, $OMnCO^-$, $OFeCO^-$, and $OCoCO^-$ molecular anions were about 200 cm^{-1} lower than the OMCO neutral molecules. From Fe to Zn, the C−O stretching frequencies increased. For $OCuCO^-$ and $OZnCO^-$, most of the negative charge remains on CuO and ZnO, which are more like OCu^-- - -CO and OZn^-- - -CO complexes.

The $OMCO^-$ anions were produced by electron capture of OMCO molecules, reaction 3, which was calculated to be exothermic for all metals. The $OMCO^-$ absorptions increased

$$OMCO + e^- \rightarrow OMCO^- \quad (3)$$

slightly on photolysis using 470 nm long-wavelength pass radiation when CO_2^- was photobleached. The $OCuCO^-$ and $OZnCO^-$ anions were probably produced by reaction of Cu and Zn with CO_2^-, as the neutral OCuCO and OZnCO molecules

TABLE 10: Comparison of Observed and Calculated Vibrational Frequencies (cm^{-1}) and Isotopic Frequency Ratios for OMCO, $OMCO^-$, and MCO_2^-

molecule	frequency observed	frequency calculated	*R*(12/13) observed	*R*(12/13) calculated	*R*(16/18) observed	*R*(16/18) calculated
OCrCO	2014.4	1995.5	1.0226	1.0234	1.0239	1.0238
	866.3	941.7	1.0000	1.0000	1.0444	1.0453
OMnCO	2082.5	2026.7	1.0226	1.0234	1.0242	1.0239
	869.9	901.0	1.0000	1.0000	1.0447	1.0455
OFeCO	2037.1	2017.8	1.0229	1.0237	1.0241	1.0235
	872.8	897.8	1.0000	1.0000	1.0455	1.0455
OCoCO	2026.6	2017.5	1.0232	1.0239	1.0232	1.0230
	783.8	853.4	1.0000	1.0000	1.0444	1.0461
ONiCO	2086.6	2054.9	1.0230	1.0239	1.0236	1.0231
		766.0		1.0000		1.0462
$OCrCO^-$	1831.1	1805.3	1.0237	1.0239	1.0226	1.0231
	825.5	848.2	1.0013	1.0000	1.0430	1.0447
$OMnCO^-$	1856.7	1783.8	1.0239	1.0244	1.0220	1.0222
	810.1	833.0	1.0000	1.0001	1.0430	1.0443
$OFeCO^-$	1806.2	1788.4	1.0243	1.0249	1.0212	1.0214
	814.8	815.0	1.0000	1.0000	1.0429	1.0443
$OCoCO^-$	1849.2	1839.0	1.0242	1.0250	1.0213	1.0213
	807.9	803.3	1.0012	1.0001	1.0438	1.0453
$ONiCO^-$	1881.4	1875.0	1.0243	1.0250	1.0212	1.0212
		736.4		1.0001		1.0431
$OCuCO^-$	1943.4	1906.4	1.0245	1.0250		1.0214
		808.5		1.0001		1.0430
$OZnCO^-$	2084.4		1.02392			
$CoCO_2^-$	1693.5	1726.2	1.0268	1.0274	1.0402	1.0182
	1228.4	1194.9	1.0115	1.0091	1.0297	1.0447
	721.9	680.1	1.0204	1.0223		1.0270
$NiCO_2^-$	1684.8	1665.9	1.0261	1.0271	1.0170	1.0187
	1226.1	1189.8	1.0116	1.0114	1.0387	1.0409
	723.9	729.4	1.0204	1.0214	1.0296	1.0285
$CuCO_2^-$	1713.4	1762.2	1.0275	1.0279		1.0175
	1234.2	1197.6	1.0112	1.0082		1.0464
	697.0	667.1	1.0209	1.0221		1.0276

TABLE 11: Calculated Vibrational Frequencies (cm^{-1}) and Intensities (km/mol) of O_2MnCO, $Mn(O)_2CO$, O_2FeCO, and $Fe(O)_2CO$ Molecules

O_2MnCO ($^4A''$)[a]	$Mn(O)_2CO$ ($^4B_2$)[b]	$Mn(O)_2CO$ ($^6A_1$)[c]	O_2FeCO ($^3A''$)[d]	$Fe(O)_2CO$ ($^5A_1$)[e]	$Fe(O)_2CO$ ($^3A_2$)[f]
2058.6(760) (A′)	1763.2(405) (A_1)	1741.5(477) (A_1)	2068.4(599) (A′)	1738.0(399) (A_1)	1753.5(418) (A_1)
942.4(173) (A″)	1000.0(154) (B_2)	943.1(393) (B_2)	961.0(145) (A″)	951.9(223) (B_2)	1005.7(185) (B_2)
936.4(43) (A′)	893.5(0.4) (A_1)	873.9(49) (A_1)	924.5(11) (A′)	872.3(27) (A_1)	904.3(23) (A_1)
435.1(14) (A′)	734.0(55) (A_1)	758.8(12) (B_1)	511.7(10) (A′)	746.4(17) (B_1)	757.1(21) (B_1)
338.7(1) (A′)	728.3(8) (B_1)	741.4(54) (A_1)	412.7(0) (A′)	737.3(54) (A_1)	711.6(44) (A_1)
310.8(1) (A″)	607.2(0) (B_2)	593.8(10) (B_2)	385.1(6) (A″)	589.6(3) (B_2)	606.2(0) (B_2)
278.2(7) (A′)	445.7(15) (A_1)	416.1(51) (A_1)	245.2(8) (A′)	400.7(34) (A_1)	461.8(35) (A_1)
120.7(26) (A′)	384.7(2) (B_2)	246.5(35) (B_2)	164.7(18) (A′)	311.5(1) (B_2)	395.6(1) (B_2)
88.9(1) (A″)	164.3(5) (B_1)	142.2(7) (B_1)	115.9(0.3) (A″)	142.9(8) (B_1)	166.7(5) (B_1)

[a] Structure: Mn−O: 1.612 Å, Mn−C: 1.922 Å, C−O: 1.146 Å, ∠OMnO: 118.8°, ∠OMnC: 109.1°, ∠MnCO: 173.4°. [b] Structure: Mn−O: 1.822 Å, O−C: 1.371 Å, C−O: 1.203 Å, ∠OMnO: 73.3°, ∠OCO: 105.0°, the $^4A''$ O_2MnCO is 2.6 kcal/mol lower in energy than $Mn(O)_2CO$ $^4B_2$ state. [c] Structure: Mn−O: 1.907 Å, O−C: 1.379 Å, C−O: 1.209 Å, ∠OMnO: 72.1°, ∠OCO: 108.9°, the $^6A_1$ state is 12.5 kcal/mol lower in energy than $^4B_2$ $Mn(O)_2CO$. [d] Structure: Fe−O: 1.602 Å, Fe−C: 1.810 Å, C−O: 1.149 Å, ∠OFeO: 127.7°, ∠OFeC: 107.3°, ∠FeCO: 173.5°. [e] Structure: Fe−O: 1.873 Å, O−C: 1.376 Å, C−O: 1.207 Å, ∠OFeO: 73.1°, ∠OCO: 108.2°. [f] Structure: Fe−O: 1.818 Å, O−C: 1.370 Å, C−O: 1.205 Å, ∠OFeO: 73.0°, ∠OCO: 104.2°. The $^5A_1$ state $Fe(O)_2CO$ is 1.3 and 4.8 kcal/mol lower in energy than $^3A''$ O_2FeCO and $^3A_2$ $Fe(O)_2CO$.

were not observed here.

$$M + CO_2^- \rightarrow OMCO^- \quad (4)$$

MCO_2^-. Weak band sets at 1693.5, 1228.4, 721.9 cm^{-1} for Co, 1684.8, 1226.1, 723.9 cm^{-1} for Ni, and 1713.4, 1234.2, 697.0 cm^{-1} for Cu were observed after deposition, decreased on annealing, and destroyed on photolysis. The Ni system will be used as an example; the 1684.8 cm^{-1} band shifted to 1641.9 and 1656.7 cm^{-1} in $^{13}C^{16}O_2$ and $^{12}C^{18}O_2$ spectra and the isotopic 12/13 ratio 1.0261 and 16/18 ratio 1.0170 indicate that this is an antisymmetric OCO vibration. The 1226.1 cm^{-1} band shifted to 1212.1 and 1180.4 cm^{-1} in $^{13}C^{16}O_2$ and $^{12}C^{18}O_2$ spectra, and the 12/13 ratio 1.0116 and 16/18 ratio 1.0387 were characteristic of a symmetric OCO vibration, the lower 723.9 cm^{-1} band has 1.0204 12/13 and 1.0296 16/18 ratios, which are appropriate for a OCO bending vibration. In mixed $^{12}C^{16}O_2 + {}^{13}C^{16}O_2$ and $^{12}C^{16}O_2 + {}^{12}C^{18}O_2$ experiments, only pure isotopic counterparts were observed for all three modes, indicating that only one CO_2 unit is involved in this molecule. These bands were eliminated in CCl_4-doped experiments, strongly suggesting an anion species. The upper mode is only tens of wavenumbers higher than the CO_2^- absorption, so the MCO_2^- anion is suggested.

DFT calculations predicted that for Co and Ni the MCO_2^- anion is slightly higher in energy than $OMCO^-$, while for Cu the $CuCO_2^-$ anion is lower in energy than $OCuCO^-$. As listed in Table 10, the calculation predicted the antisymmetric OCO, symmetric OCO, and bending modes of the MCO_2^- anions in excellent agreement with the observed values.

The MCO_2^- anions were produced by addition reaction 5

$$M + CO_2^- \rightarrow MCO_2^- \quad (5)$$

O_2MnCO and O_2FeCO. A weak band in the Mn + CO_2 system was produced at 2097.3 cm^{-1} on full-arc photolysis; this band showed C−O stretching vibrational ratios (12/13: 1.0233, 16/18:1.0231), and only doublets were observed in mixed $^{12}C^{16}O_2 + {}^{13}C^{16}O_2$ and $^{12}C^{16}O_2 + {}^{12}C^{16,18}O_2 + {}^{12}C^{18}O_2$ experiments. This band is assigned to the O_2MnCO molecule, and unfortunately the MnO_2 stretching vibrations are too weak to be observed here. In the Fe + CO_2 system, two bands at 2108.2 and 1005.9 cm^{-1} grew together on annealing; the upper band has C−O stretching vibrational ratios, and only one CO submolecule is involved. The 1005.9 cm^{-1} band showed the characteristic antisymmetric OFeO ratio,[30] and the 1/2/1 triplet in the mixed $^{12}C^{16}O_2 + {}^{12}C^{16,18}O_2 + {}^{12}C^{18}O_2$ experiment confirmed the involvement of two equivalent O atoms. These two bands are assigned to the O_2FeCO complex. The symmetric OFeO vibration is too weak to be observed here. A similar O_2-FeNN complex has been observed at 2271.3 and 1002.0 cm^{-1}.[30]

$Mn(O)_2CO$ and $Fe(O)_2CO$. In the Mn + CO_2 system, weak bands at 1755.4, 1077.0, and 772.7 cm^{-1} markedly increased together on annealing, indicating that these bands are due to different modes of the same molecule. The 1755.4 cm^{-1} band showed C−O stretching vibrational isotopic ratios (12/13: 1.0229, 16/18:1.0218) and only doublets in mixed $^{12}C^{16}O_2 + {}^{13}C^{16}O_2$ and $^{12}C^{16}O_2 + {}^{12}C^{16,18}O_2 + {}^{12}C^{18}O_2$ experiments, which means that only one CO subunit is involved in this mode. The 1077.0 cm^{-1} band exhibited a large 12/13 ratio (1.0266) and a small 16/18 ratio (1.0174). In the mixed $^{12}C^{16}O_2 + {}^{13}C^{16}O_2$ experiment, a doublet was observed, while in the $^{12}C^{16}O_2 + {}^{12}C^{16,18}O_2 + {}^{12}C^{18}O_2$ spectrum, a sextet was produced; this sextet actually was a 1/2/1 triplet of doublets, suggesting two equivalent oxygen atoms slightly perturbed by another inequivalent oxygen atom. A similar sextet was observed for the 772.7 cm^{-1} band, which confirms that this molecule incorporates a CO_3 subunit. $Mn(O)_2CO$ was first considered. DFT calculations predicted that the $Mn(O)_2CO$ molecule is close in energy with another O_2MnCO isomer that is also observed here. As listed in Table 11, the calculated frequencies of three modes are in very good agreement with the observed values, and the calculated isotopic ratios are also very close to the observed values.

A similar band set at 1767.8, 1031.5, 907.8, 793.6, and 791.3 cm^{-1} was observed in the Fe + CO_2 system and is assigned to the $Fe(O)_2CO$ molecule. Here, five modes were observed, as the calculation also predicted (Table 11).

The O_2MnCO and O_2FeCO complexes were produced by reaction of MnO_2 and FeO_2 with CO, reaction 6, while the $Mn(O)_2CO$ and $Fe(O)_2CO$ molecules were probably produced by reaction of MnO and FeO with CO_2, reaction 7.

$$MO_2 + CO \rightarrow O_2MCO \quad (6)$$

$$MO + CO_2 \rightarrow M(O)_2CO \quad (7)$$

No obvious bands in the Co, Ni, and Cu systems can be assigned to similar O_2MCO and $M(O)_2CO$ molecules, as the needed MO_2 and MO absorptions were weak in these systems.

$O_2Mn(CO)_2$. Three bands at 2126.0, 2056.0, and 993.8 cm^{-1} tracked in all the experiments. The 993.8 cm^{-1} absorption showed no carbon-13 shift, but the 16/18 ratio 1.0386 indicated an antisymmetric MnO_2 vibration. Both the 2056.0 and 2126.0 cm^{-1} bands exhibited terminal C−O stretching vibrational isotopic ratios, and triplets were observed in both $^{12}C^{16}O_2 + {}^{13}C^{16}O_2$ and $^{12}C^{16}O_2 + {}^{12}C^{16,18}O_2 + {}^{12}C^{18}O_2$ spectra, which are suitable for antisymmetric and symmetric C−O vibrations of a $Mn(CO)_2$ subunit. Analogous to the $O_2Cr(CO)_2$ and $O_2V(CO)_2$ molecules, these three bands were assigned to the $O_2Mn(CO)_2$ molecule.

Cation Absorptions. In the Mn + CO_2 system, two bands at 2173.0 and 851.9 cm^{-1} increased on photolysis and 30 K annealing: the upper band is due to a C−O stretching vibration, while the lower band showed the terminal Mn−O stretching isotopic ratio. Doublet structures in mixed $^{12}C^{16}O_2 + {}^{13}C^{16}O_2$ and $^{12}C^{16}O_2 + {}^{12}C^{16,18}O_2 + {}^{12}C^{18}O_2$ experiments suggested one CO and one O involvement in the upper and lower modes, respectively. These two bands are in excellent agreement with calculated values (2204.3, 967.1 cm^{-1}, Table 5), which supports assignment to the $OMnCO^+$ cation. The relative yield of $OMnCO^+$ to OMnCO increases two-fold with CCl_4 doping, which supports the cation identification. Note that the scale factor (observed/calculated) for the C−O stretching mode (0.986) is in accord with values expected for BP86 calculations,[38] but the scale factor for the Mn−O stretching mode (0.881) is much lower. Clearly the C−O bond is easier to model theoretically than the Mn−O bond.

The weaker 2175.5 cm^{-1} band assigned previously[22] to a combination band of OCrCO is here reassigned to the $OCrCO^+$ cation. This band exhibits isotopic frequency ratios (12/13, 1.0229; 16/18, 1.0238) that are almost the same as the OCrCO band at 2014.4 cm^{-1} (Table 10) and is intermediate between the C−O stretching modes for $OMnCO^+$ (2173.0 cm^{-1}) and $OVCO^+$ (2205.4 cm^{-1}).[21]

Analogous bands at 2079.1, 885.6 cm^{-1} in the Fe + CO_2 system and 2081.6, 854.1 cm^{-1} in the Co + CO_2 system exhibited a similar behavior and are tentatively assigned to the $FeOCO^+$ and $CoOCO^+$ molecular cations, which are essentially MO^+- - -CO. Note that the frequencies are lower than the C−O fundamental. We also note that FeO^+- - -CO is higher energy than the Fe^+- - -OCO complex calculated earlier.[17] The latter complex, if produced here, cannot be observed because the perturbed OCO modes are masked by CO_2 absorption.

The 2229.5 cm^{-1} band in zinc experiments is probably due to the analogous ZnO^+- - -CO cation complex where ZnO^+ extensively polarizes the CO subunit.

Conclusions

Laser-ablated Cr through Ni atoms react with CO_2 molecules to give the insertion product, OMCO, which have been isolated in solid argon matrices. The $OMCO^-$ insertion molecular anions (Cr through Zn) were formed by electron capture and/or reaction with CO_2^-, and the MCO_2^- anions (M = Co, Ni, Cu) were produced by the addition of metal atoms to CO_2^-, also formed by electron capture in these experiments.

The excellent agreement with frequencies and isotopic frequency ratios from density functional calculations support the vibrational assignments and the identification of these transition metal species.

The C−O stretching frequencies for OMCO and $OMCO^-$ are predicted within 1% for all metals but Mn, which are within 3%. The M−O stretching modes are predicted less accurately within 3−9% for all metals. Clearly the transition metal−oxygen bond is more difficult to model theoretically than the C−O bond.

Acknowledgment. The authors thank the National Science Foundation (Grant No. CHE97-00116) for support of this work.

References and Notes

(1) Palmer, D. A.; Van Eldik, R. *Chem. Rev.* **1983**, *83*, 651.
(2) Solymosi, F. *J. Mol. Catal.* **1991**, *65*, 337.

(3) Creutz, C. In *Electrochemical and Electrocatalytic Reactions of Carbon Dioxide*; Sullivan, B. P., Krist, K., Guard, H. E., Eds.; Elsevier: Amsterdam, 1993.
(4) Gibson, D. H. *Chem. Rev.* **1996**, *96*, 2063.
(5) Huber, H.; McIntosh, D.; Ozin, G. A. *Inorg. Chem.* **1977**, *16*, 495.
(6) Ozin, G. A.; Huber, H.; McIntosh, D. *Inorg. Chem.* **1978**, *17*, 147.
(7) Mascetti, J.; Tranquille, M. *J. Phys. Chem.* **1988**, *92*, 2173.
(8) Sievers, M. R.; Armentrout, P. B. *J. Chem. Phys.* **1995**, *102*, 754.
(9) Schwarz, J.; Heinemann, C.; Schwarz, H. *J. Phys. Chem.* **1995**, *99*, 11405.
(10) Asher, R. L.; Bellert, D.; Buthelezi, T.; Brucat, P. J. *Chem. Phys. Lett.* **1994**, *227*, 623.
(11) Baranov, V.; Javahery, G.; Hophinson, A. C.; Bohme, D. K. *J. Am. Chem. Soc.* **1995**, *117*, 12801.
(12) Galan, G.; Fouassier, M.; Tranquille, M.; Mascetti, J.; Papai, I. *J. Phys. Chem. A* **1997**, *101*, 2626.
(13) Jeung, G. *Mol. Phys.* **1989**, *67*, 747.
(14) Caballol, R.; Sanchez Marcos, E.; Barthelat, J. C. *J. Phys. Chem.* **1987**, *91*, 1328.
(15) Sodupe, M.; Branchadell, V.; Oliva, A. *J. Phys. Chem.* **1995**, *99*, 8567.
(16) Sodupe, M.; Branchadell, V.; Oliva, A. *J. Mol. Struct.* **1996**, *371*, 79.
(17) Sodupe, M.; Branchadell, V.; Rosi, M.; Bauchlicher, C. W., Jr. *J. Phys. Chem. A* **1997**, *101*, 1854.
(18) Papai, I.; Mascetti, J.; Fournier, R. *J. Phys. Chem. A* **1997**, *101*, 4465.
(19) Chertihin, G. V.; Andrews, L. *J. Am. Chem. Soc.* **1995**, *117*, 1595.
(20) Zhou, M.; Andrews, L. *J. Am. Chem. Soc.* **1998**, *120*, 13230.
(21) Zhou, M.; Andrews, L. *J. Phys. Chem. A* **1999**, *103*, 2066. (V and Ti + CO_2).
(22) Souter, P. F.; Andrews, L. *J. Am. Chem. Soc.* **1997**, *119*, 7350.
(23) Burkholder, T. R.; Andrews, L. *J. Chem. Phys.* **1991**, *95*, 8697.
(24) Hassanzadeh, P.; Andrews, L. *J. Phys. Chem.* **1992**, *96*, 9177.
(25) Jacox, M. E.; Thompson, W. E. *J. Chem. Phys.* **1989**, *91*, 1410.
(26) Zhou, M.; Andrews, L. *J. Chem. Phys.* **1999**, *110*, 2414.
(27) Zhou, M.; Andrews, L. *J. Chem. Phys.* **1999**, in press. ($C_2O_4^+$).
(28) Jacox, M. E.; Thompson, W. E. *J. Phys. Chem.* **1991**, *95*, 2781.
(29) Chertihin, G. V.; Andrews, L. *J. Phys. Chem. A* **1997**, *101*, 8547.
(30) Chertihin,G. V.; Saffel, W.; Yustein, J. T.; Andrews, L.; Neurock, M.; Ricca, A.; Bauschlicher, C. W., Jr. *J. Phys. Chem.* **1996**, *100*, 5261.
(31) Chertihin, G. V.; Cita, A.; Andrews, L.; Bauschlicher, C. W., Jr. *J. Phys. Chem. A* **1997**, *101*, 8793; Citra, A.; Chertihin, G. V.; Andrews, L.; Newrock, M. *J. Phys. Chem. A* **1997**, *101*, 3109.
(32) Jacox, M. E.; Milligan, D. E. *J. Chem. Phys.* **1971**, *54*, 3935.
(33) Prochaska, F. T.; Andrews, L. *J. Chem. Phys.* **1977**, *67*, 1091 and references therein.
(34) Frisch, M. J.; Trucks, G. W.; Schlegel, H. B.; Gill, P. M. W.; Johnson, B. G.; Robb, M. A.; Cheeseman, J. R.; Keith, T.; Petersson, G. A.; Montgomery, J. A.; Raghavachari, K.; Al-Laham, M. A.; Zakrzewski, V. G.; Ortiz, J. V.; Foresman, J. B.; Cioslowski, J.; Stefanov, B. B.; Nanayakkara, A.; Challacombe, M.; Peng, C. Y.; Ayala, P. Y.; Chen, W.; Wong, M. W.; Andres, J. L.; Replogle, E. S.; Gomperts, R.; Martin, R. L.; Fox, D. J.; Binkley, J. S.; Defrees, D. J.; Baker, J.; Stewart, J. P.; Head-Gordon, M.; Gonzalez, C.; Pople, J. A. *Gaussian 94, Revision B.1*; Gaussian, Inc.: Pittsburgh, PA, 1995.
(35) Perdew, J. P. *Phys. Rev. B* **1986**, *33*, 8822. Becke, A. D. *J. Chem. Phys.* **1993**, *98*, 5648.
(36) McLean, A. D.; Chandler, G. S. *J. Chem. Phys.* **1980**, *72*, 5639. Krishnan, R.; Binkley, J. S.; Seeger, R.; Pople, J. A. *J. Chem. Phys.* **1980**, *72*, 650.
(37) Wachters, J. H. *J. Chem. Phys.* **1970**, *52*, 1033. Hay, P. J. *J. Chem. Phys.* **1977**, *66*, 4377.
(38) Scott, A. P.; Radom, L. *J. Phys. Chem.* **1996**, *100*, 16502.